JOURNAL OF SOLID STATE CHEMISTRY 77, 348–355 (1988)

Preparation and Transport Properties of the Substituted Blue Bronze $(Rb_{1-x}Cs_x)_{0.3}MoO_3$

B. T. COLLINS, K. V. RAMANUJACHARY, AND M. GREENBLATT*

Department of Chemistry, Rutgers, The State University of New Jersey, New Brunswick, New Jersey 08903

AND J. V. WASZCZAK

AT&T, Bell Laboratories, Murray Hill, New Jersey 07974

Received May 26, 1988; in revised form August 8, 1988

Electrical and magnetic transport properties have been measured on single crystals of the molybdenum blue bronze alloy system $(Rb_{1-x}Cs_x)_{0.3}MoO_3$ prepared by the temperature gradient flux technique. Although the properties of the blue bronze are retained, cesium substitution decreases both ρ (298 K) and the transition temperature observed at 180 K for $Rb_{0.3}MoO_3$. Solid-state studies indicate that the upper limit of Cs doping is approximately 45%. Attempts are made to correlate the effects of cesium substitution with the observed changes in the transport properties.

Introduction

The alkali metal molybdenum oxide bronzes with general formula $A_{0.3}MoO_3$ (A = K, Tl, Rb) have been intensively investigated since the discovery of quasi-one-dimensional metallic properties in $K_{0.3}MoO_3$ at room temperature (*1*). Shortly thereafter, X-ray diffuse scattering studies on $K_{0.3}MoO_3$ and $Rb_{0.3}MoO_3$ confirmed that the metal–semiconductor transition observed at 180 K was due to a charge-density wave (CDW) instability (*2*). The appearance of nonlinear conductivity at relatively low applied dc fields (*3, 4*), increased ac conductivity at low frequencies (*5*), and memory and hysteresis effects (*6*) have all been attributed to charge-transport via a "sliding" or moving CDW. The structure of the so-called "blue bronzes" consists of infinite layers of edge- and corner-sharing MoO_6 octahedra held together by the A cations (*7–9*). Although the bonding is three-dimensional (3D), the properties are quasi-one-dimensional (1D) because the 4*d* electrons are located mainly on the Mo sites involved in infinite chains of MoO_6 octahedra parallel to the *b*-axis of the monoclinic unit cell (*8*).

Recently, Schneemeyer *et al.* (*10*) reported on the alloy systems $(K_{1-x}Rb_x)_{0.3}MoO_3$ and $K_{0.3}Mo_{1-x}W_xO_3$. They reported dramatic impurity effects on the charge-density wave dynamics with substitution of these isoelectronic dopants (*11, 12*).

For the past few years our group has

* To whom correspondence should be addressed.

0022-4596/88 $3.00

been involved with preparing single-crystal specimens of the molybdenum oxide bronzes by a temperature gradient flux technique (TGFT) (*13*, *14*). More recently, we have been studying the effects of substitutions on the electrical and magnetic properties of these phases. We have examined the change in the properties of the low-dimensional purple bronze $Li_{0.9}Mo_6O_{17}$ by doping of Na for Li and W for Mo, respectively (*15*). In addition, we have looked at the effects of vanadium substitution on the semiconducting, anisotropic bronze, $Li_{0.33}Mo_{1-x}V_xO_3$ (*16*).

In this work we describe the substituted blue bronze phase $(Rb_{1-x}Cs_x)_{0.3}MoO_3$. The pure blue bronze, $Cs_{0.3}MoO_3$, is not known to exist, apparently as a result of the large size of Cs^+. Quite surprisingly, we have been able to substitute large amounts of cesium (~45%) into the $Rb_{0.3}MoO_3$ structure. In this paper, we describe the preparation of $(Rb_{1-x}Cs_x)_{0.3}MoO_3$ single crystals along with the structural, electronic, and magnetic properties of these phases.

Experimental

Single crystals of $(Rb_{1-x}Cs_x)_{0.3}MoO_3$ were grown by the temperature gradient flux technique (TGFT). Stoichiometric quantities of the reactants were weighed out according to the equation

$$n(1-x)Rb_2MoO_4 + nxCs_2MoO_4 + 2(1-n)MoO_3 + nMoO_2 = 2(Rb_{1-x}Cs_x)_nMoO_3,$$

where $0.3 \leq n \leq 0.4$ and $0 \leq x \leq 0.75$.

Polycrystalline samples of $(Rb_{1-x}Cs_x)_{0.3}MoO_3$ were also prepared. Samples with $x < 0.325$ were prepared at 550°C (96 hr, 1 regrinding). Samples with $x > 0.325$ undergo partial melting when heated directly to 550°C. Therefore, these samples were first heated to 505°C (48 hr), reground, and heated to 550°C (48 hr). All reactions were carried out in evacuated silica tubes according to the equation

$$0.3(1-x)Rb_2MoO_4 + 0.3xCs_2MoO_4 + 1.4MoO_3 + 0.3MoO_2 = 2(Rb_{1-x}Cs_x)_{0.3}MoO_3,$$

where $0 \leq x \leq 0.45$.

Rb_2MoO_4 and Cs_2MoO_4 were prepared by heating stoichiometric mixtures of Rb_2CO_3 (AESAR, 99.9%) or Cs_2CO_3 (AESAR, 99.9%) and reagent-grade MoO_3 (J. T. Baker) in air at 750 and 850°C, respectively, for ~15 hr with at least 1 regrinding. MoO_2 (ROC/RIC) which had a stated purity of 99.9% was washed several times with alternate portions of hot, dilute HCl, water, and ammonia to remove traces of molybdenum blue.

The $(Rb_{1-x}Cs_x)_{0.3}MoO_3$ crystals were dark blue rectangular platelets. Samples selected for study had typical dimensions 2–4 × 1 × 0.5 mm^3. Cell parameters were obtained by least-squares analysis of powder data obtained with a Scintag PAD V automated diffractometer employing monochromatic Cu$K\alpha$ radiation. Silicon was used as an internal standard.

Chemical analysis for Rb and Mo was determined by plasma emission spectroscopy. Rb and Cs analysis was obtained with atomic absorption spectroscopy. The orientation of selected crystals was determined by oscillation photography. Low-temperature (between 77 and 298 K) electrical resistivity measurements were made employing a four-probe configuration using ultrasonically soldered indium contacts in a conventional liquid helium cryostat. On average, contact resistances at room temperature were between 0.5 and 3 Ω for current parallel to *b* and between 1 and 10 Ω for current perpendicular to *b* and the (201) cleavage plane. Magnetic susceptibility from 4.2 to 298 K was performed on randomly oriented single crystals by the Faraday method (*17*).

TABLE I

SUMMARY OF THE EXPERIMENTAL CONDITIONS AND BRONZE CRYSTAL FORMATION

$(Rb_{1-x}Cs_x)_nMoO_3$			Temperature gradient			
Sample	n	x	$T_{0\,cm}$ (°C)	$T_{6\,cm}$ (°C)	$T_{14\,cm}$ (°C)	Bronze phases
Rb-1	0.3	0	585	565	535	Only blue bronze crystals 4–6 mm long
RbCs-1	0.3	0.25	585	569	530	Only blue bronze crystals 3–4 mm long
RbCs-2	0.3	0.75	569	539	498	Polycrystalline $Cs_{0.33}MoO_3$ and blue bronze crystals 0.5–1 mm long
RbCs-3	0.4	0.25	579	565	522	Polycrystalline $Cs_{0.33}MoO_3$ and blue bronze crystals up to 6 mm long
RbCs-4	0.4	0.50	551	540	503	Only $Cs_{0.33}MoO_3$ crystals up to 2.5 mm long
RbCs-5	0.4	0.75	561	545	501	Only $Cs_{0.33}MoO_3$ crystals 3–4 mm long
RbCs-6	0.4	0.50	568	552	511	Both blue and red bronze crystals up to 5 mm long
RbCs-7	0.3	0.25	608	588	546	Only blue bronze crystals up to 7 mm long
RbCs-8	0.3	0.50	590	570	526	Only blue bronze crystals up to 4 mm long
RbCs-9	0.3	0.75	590	570	526	Blue bronze crystals (up to 1.5 mm long) with some red bronze intergrowth
RbCs-10	0.3	0.75	583	565	527	Polycrystalline $Cs_{0.33}MoO_3$ and blue bronze crystals up to 1.5 mm long
RbCs-11	0.3	0.75	568	555	515	Red and blue bronze intergrowth and blue bronze crystals 0.5–2 mm long

Results

Crystal Growth

For the preparation of $(Rb_{1-x}Cs_x)_{0.3}MoO_3$ blue bronze crystals by the TGFT both the nominal composition and the reaction temperature are of utmost importance. It was reported earlier (*14*) that the growth of pristine $Rb_{0.3}MoO_3$ is optimized with starting stoichiometry Rb_nMoO_3 ($0.30 \leq n \leq 0.35$). The red bronze, $Rb_{0.33}MoO_3$, has never been prepared by the temperature gradient flux technique. However, large crystals of the red bronze, $Cs_{0.33}MoO_3$, are found for nominal compositions Cs_nMoO_3 ($0.35 \leq n \leq 0.40$).

Listed in Table I is a summary of the experimental conditions for the preparation of mixed bronze crystals of composition $(Rb_{1-x}Cs_x)_{0.3}MoO_3$. Noteworthy observations are (1) for $n = 0.3$ only blue bronze crystals are found (even for $x = 0.75$); (2) for $n = 0.3$ and $x = 0.75$ the amount of polycrystalline $Cs_{0.33}MoO_3$ increases with decreased reaction temperature; (3) when $n = 0.3$ and $x = 0$, 0.25, and 0.50 the crystal size is markedly larger than when $x = 0.75$; (4) if $n = 0.4$ and $x = 0.75$, only red bronze crystals are formed; (5) for $n = 0.4$ and $x = 0.25$ small blue bronze crystals are present; and (6) for $n = 0.4$ and $x = 0.5$ both blue and red bronze crystals form with the former favored with increasing temperature.

Chemical Analysis

Table II gives the results of chemical analysis on selected blue bronze crystals. The reliability of rubidium analysis by plasma emission spectroscopy was checked by examining unsubstituted $Rb_{0.3}MoO_3$ for Rb and Mo content. As shown in Table II a value of $Rb_{0.294}MoO_3$ was obtained which is within the expected 2% experimental error. The results obtained for Rb and Cs analysis by atomic absorption spectroscopy are listed under the weight percentage formula.

TABLE II

CHEMICAL ANALYSIS RESULTS FOR SELECTED BLUE BRONZE CRYSTALS

	Atomic absorption spectroscopy		Plasma emission
Sample	Weight % formula	Standard formula	(0.3 − Rb content = Cs content)
Rb-1	$Rb_{0.323}MoO_3$	$Rb_{0.3}MoO_3$	$Rb_{0.294}MoO_3$
RbCs-3	—	—	$(Rb_{0.887}Cs_{0.113})_{0.3}MoO_3$
RbCs-6	—	—	$(Rb_{0.683}Cs_{0.317})_{0.3}MoO_3$
RbCs-7	$Rb_{0.314}Cs_{0.041}MoO_3$	$(Rb_{0.883}Cs_{0.117})_{0.3}MoO_3$	$(Rb_{0.833}Cs_{0.167})_{0.3}MoO_3$
RbCs-8	$Rb_{0.223}Cs_{0.125}MoO_3$	$(Rb_{0.640}Cs_{0.360})_{0.3}MoO_3$	$(Rb_{0.623}Cs_{0.377})_{0.3}MoO_3$
RbCs-11[a]	—	—	$(Rb_{0.413}Cs_{0.587})_{0.3}MoO_3$

[a] Not pure, red bronze intergrowth.

Consistently high alkali metal content is observed, e.g., $Rb_{0.323}MoO_3$ instead of $Rb_{0.3}MoO_3$. Normalized data (total alkali metal content equal to 0.3) is tabulated under standard formula. The normalized results follow the same trend as plasma emission analysis with the total alkali content assumed to be 0.3.

Dumas *et al.* (*18*) recently reported that crystals of $K_{0.3}MoO_3$ grown by a flux technique have higher alkaline concentration then electrolytically grown samples based on microprobe analysis. However, plasma emission on TGFT-prepared $Rb_{0.3}MoO_3$ indicates little, if any deviation from ideal stoichiometry. It is apparent, as will be discussed subsequently, that 45% of the rubidium can be replaced with cesium while maintaining the integrity of the blue bronze structure.

Cell Parameters

Unit cell parameters for the $(Rb_{1-x}Cs_x)_{0.3}MoO_3$ single crystals and polycrystalline samples were calculated by least-squares analysis of 20 to 30 selected reflections between 5 and 45° 2θ.

Table III and Fig. 1 indicate that the upper limit for Cs doping is ~45%. The cell volume changes little for larger substitution levels. Above 45% substitution, there are other phases present in addition to the Rb–Cs blue bronze (e.g., $Cs_{0.33}MoO_3$). Also, the monoclinic *b* axis remains nearly constant for all amounts of cesium substitution.

Attempts to calculate cell parameters for red bronze crystals prepared by the TGFT were unsuccessful. It was difficult to ascertain from the data whether Rb was replacing Cs in $Cs_{0.33}MoO_3$. There was little, if any, decrease in the cell volume and the standard deviations were quite large. This avenue was not pursued further.

Electrical Resistivity

The electrical transport properties were measured on a large number of $(Rb_{1-x}Cs_x)_{0.3}MoO_3$ crystals. As has been noted (*19*),

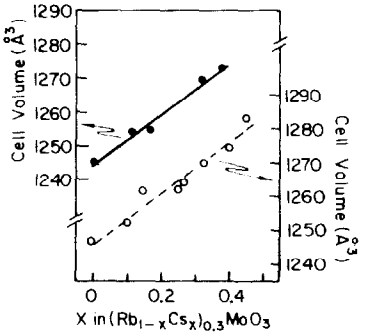

FIG. 1. Variation of the cell volume as a function of Cs content in $(Rb_{1-x}Cs_x)_{0.3}MoO_3$; ●, temperature gradient flux grown crystals (solid line); ○, solid-state reactions (dashed line).

TABLE III

CELL PARAMETERS FOR $(Rb_{1-x}Cs_x)_{0.3}MoO_3$ PHASES

Sample	Composition	Space group	a (Å)	b (Å)	c (Å)	β (°)	V (Å^3)
			TGFT Crystals				
Single[a] crystal	$Rb_{0.3}MoO_3$	$C2/m$	18.635	7.5550	10.094	118.842	1244.8
Rb-1	$Rb_{0.294}MoO_3$	$C2/m$	18.646(7)	7.545(4)	10.098(3)	118.87(2)	1244.0(7)
RbCs-3	$(Rb_{0.887}Cs_{0.113})_{0.3}MoO_3$	$C2/m$	18.739(3)	7.557(2)	10.136(2)	119.13(1)	1253.8(3)
RbCs-7	$(Rb_{0.833}Cs_{0.167})_{0.3}MoO_3$	$C2/m$	18.734(4)	7.559(2)	10.133(2)	119.08(2)	1254.1(4)
RbCs-6	$(Rb_{0.683}Cs_{0.317})_{0.3}MoO_3$	$C2/m$	18.892(6)	7.560(2)	10.210(2)	119.57(3)	1268.4(6)
RbCs-8	$(Rb_{0.623}Cs_{0.377})_{0.3}MoO_3$	$C2/m$	18.917(4)	7.565(2)	10.226(2)	119.60(2)	1272.4(5)
RbCs-11	$(Rb_{0.413}Cs_{0.587})_{0.3}MoO_3$[b]	$C2/m$	19.004(15)	7.571(5)	10.290(9)	119.78(5)	1285.01(11)
			Solid-state reactions				
1	$Rb_{0.3}MoO_3$	$C2/m$	18.649(5)	7.561(4)	10.094(3)	118.84(2)	1246.8(5)
18A	$(Rb_{0.9}Cs_{0.1})_{0.3}MoO_3$	$C2/m$	18.722(5)	7.561(2)	10.127(2)	119.14(2)	1252.1(4)
2	$(Rb_{0.85}Cs_{0.15})_{0.3}MoO_3$	$C2/m$	18.808(6)	7.554(2)	10.186(5)	119.39(3)	1261.0(5)
3	$(Rb_{0.75}Cs_{0.25})_{0.3}MoO_3$	$C2/m$	18.823(4)	7.560(2)	10.178(2)	119.39(2)	1261.8(4)
9	$(Rb_{0.733}Cs_{0.267})_{0.3}MoO_3$	$C2/m$	18.848(5)	7.562(2)	10.182(3)	119.42(2)	1264.0(4)
14B	$(Rb_{0.675}Cs_{0.325})_{0.3}MoO_3$	$C2/m$	18.898(8)	7.556(3)	10.217(4)	119.50(3)	1269.8(7)
15B	$(Rb_{0.6}Cs_{0.4})_{0.3}MoO_3$	$C2/m$	18.936(6)	7.568(4)	10.249(4)	119.80(4)	1274.5(9)
16B	$(Rb_{0.55}Cs_{0.45})_{0.3}MoO_3$	$C2/m$	19.015(6)	7.567(2)	10.281(2)	119.89(2)	1282.6(5)
19A	$(Rb_{0.5}Cs_{0.5})_{0.3}MoO_3$	$C2/m$	18.990(7)	7.559(3)	10.279(3)	119.92(2)	1278.9(6)

[a] From Ref. (*8*).
[b] Not pure, red bronze intergrowth.

samples prepared by the TGFT have broader transitions than those grown electrolytically. Presumably, this behavior is due to a large concentration of impurities and/or defects introduced during crystal growth.

Three general trends have been observed. As more cesium is incorporated into the structure the metal–semiconductor transition temperature (T_{ms}) decreases slightly (Table IV). $Rb_{0.3}MoO_3$ has $T_{ms} \sim 180$ K, whereas $(Rb_{0.623}Cs_{0.377})_{0.3}MoO_3$ has $T_{ms} \sim 168$ K (Fig. 2). With increased Cs content, for current along b, ρ (298 K) decreases (Table IV). The ratio of ρ (298 K) perpendicular to b and $(\bar{2}01)$ to ρ (298 K) parallel to b increases with cesium content.

The behavior observed shows a strong

TABLE IV

RESISTIVITY AT 298 K FOR SEVERAL $(Rb_{1-x}Cs_x)_{0.3}MoO_3$ TGFT CRYSTALS

Sample	% Cs	ρ_b (Ω cm)	$\rho_{\perp b,(\bar{2}01)}$ (Ω cm)	$\rho_{\perp b,(\bar{2}01)}/\rho_b$	T_{ms} (K)
Rb-1	0	3.00×10^{-2}	1.30	40	180
RbCs-3	11.3	1.40×10^{-2}	—	—	174
RbCs-7	16.7	1.00×10^{-2}	0.90	90	172
RbCs-8	37.7	0.18×10^{-2}	0.54	300	168
RbCs-11[a]	(58.7)	(0.33×10^{-2})	(2.02)	(600)	—

[a] Not pure, red bronze intergrowth.

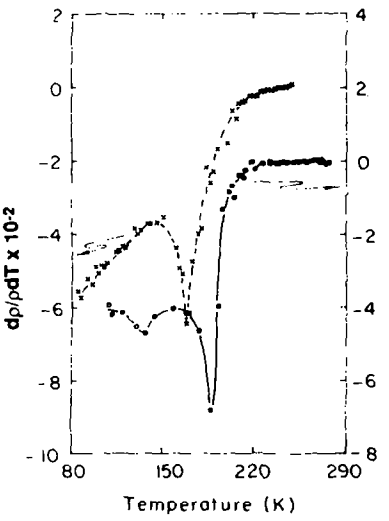

FIG. 2. $\rho^{-1}d\rho/dT$ versus temperature for $Rb_{0.3}MoO_3$ (solid line) and $(Rb_{0.623}Cs_{0.377})_{0.3}MoO_3$ (dashed line) for current parallel with b between 298 and 77 K.

sample dependence. Even for samples from the same preparation there are differences. All samples show semiconducting behavior below 180 K. Some samples display increasing resistance with decreasing temperature starting at room temperature. In addition, several samples have transitions that are so broad that a transition temperature cannot be unambiguously determined from a $\rho^{-1}d\rho/dT$ plot.

Magnetic Susceptibility

The magnetic susceptibility of randomly oriented crystals of unsubstituted $Rb_{0.3}MoO_3$ and $(Rb_{0.623}Cs_{0.377})_{0.3}MoO_3$ have been measured by the Faraday method (*17*). The data are presented with the Curie contributions substracted out. The transition observed in χ is sharper in $Rb_{0.3}MoO_3$ than in the cesium substituted sample (Fig. 3). In addition to the broadened transition, $(Rb_{0.623}Cs_{0.377})_{0.3}MoO_3$ has a decreased transition temperature compared to unsubstituted rubidium blue bronze: ~168 K versus 180 K, respectively. Both samples show a paramagnetic signal with a small temperature dependence from room temperature to ~200 K (Fig. 3, inset). $Rb_{0.3}MoO_3$ becomes diamagnetic near 164 K whereas the 37.7% Cs-doped sample is diamagnetic below 180 K. This result is due to the larger diamagnetic contribution associated with Cs as compared to Rb. The magnetic behavior is similar to that found for $Tl_{0.3}MoO_3$ (*18*) and $K_{0.3}MoO_3$ (*20*). The anomaly sometimes observed near 50 K is of unknown origin.

Discussion

The TGFT has been used to prepare large single crystals of the substituted blue bronze $(Rb_{1-x}Cs_x)_{0.3}MoO_3$. Since the amount of Cs substitution is difficult to control by the TGFT, solid-state preparations have been carried out to determine the upper limit of Cs doping. Although pure $Cs_{0.3}MoO_3$ is not known to exist, it is possible to dope large amounts of cesium (45%) into the rubidium blue bronze.

The blue bronze structure consists of slabs of MoO_6 octahedra that edge- and corner-share along the [010] and [102] directions (*7–9*). The alkali metal ions lie between the slabs holding them together. There are three crystallographically unique

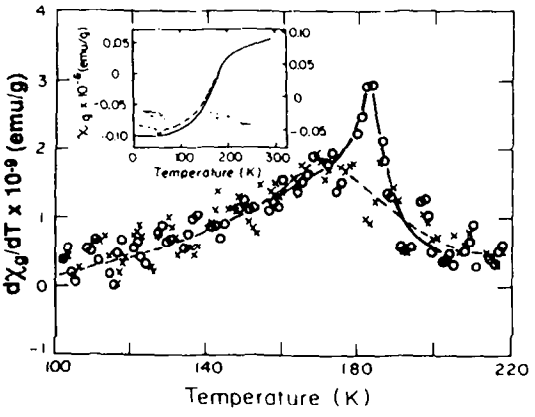

FIG. 3. $d\chi/dT$ versus temperature for $Rb_{0.3}MoO_3$ (○, solid line) and $(Rb_{0.623}Cs_{0.377})_{0.3}MoO_3$ (×, dashed line) between 220 and 100 K. Inset: χ_g versus temperature for $Rb_{0.3}MoO_3$ (solid line) and $(Rb_{0.623}Cs_{0.377})_{0.3}MoO_3$ (dashed line).

molybdenum sites. Although structurally three-dimensional, the blue bronzes are electronically one-dimensional with the 4*d* electrons being primarily located on the Mo(2) and Mo(3) sites. These sites are involved in the infinite chains of corner/edge-sharing MoO_6 octahedra along the *b* direction. In one-dimensional conductors a coupled instability of $2k_f$ of the conduction electrons and phonons leads to the formation of a CDW (*21*). It is well-established that the metal–semiconductor transition observed in the blue bronzes at 180 K is due to the formation of a CDW (*2*). The decrease in the magnetic susceptibility below ~180 K results from the loss of Fermi surface by the formation of gaps associated with the CDW transition.

Schneemeyer *et al.* (*10*) reported that the effects of alkali disorder on the transport properties of $(K_{1-x}Rb_x)_{0.3}MoO_3$ are small since the conduction band is made up of a combination of Mo dt_{2g} and O $p\pi$ orbitals. Substitution on the alkali sites should have little effect on the orbital overlap along the *b* direction in these quasi-one-dimensional compounds. For example, in changing composition from $Rb_{0.3}MoO_3$ to $(Rb_{0.5}K_{0.5})_{0.3}MoO_3$ the transition temperature changes only about 12° (decreasing from 180 to ~168 K, respectively). This decrease is observed from both $\rho^{-1}d\rho/dT$ and $d\chi_g/dT$ plots.

As expected, tungsten substitution has a strongly perturbing effect on the transport properties in the alloy system $K_{0.3}Mo_{1-x}W_xO_3$ (*10*). W disrupts the Mo dt_{2g}-O $p\pi$ overlap causing a large increase in the resistivity, a significant lowering of the transition temperature at low doping levels, and a pronounced broadening of the peaks in the derivative resistivity and magnetic susceptibility plots. By 3% tungsten doping, only semiconducting temperature dependence is observed (*10*).

Similar effects should be observed in the $(Rb_{1-x}Cs_x)_{0.3}MoO_3$ and $(Rb_{1-x}K_x)_{0.3}MoO_3$ systems since presumably only disorder in the alkali sublattice is being introduced. As the concentration of Cs is increased, T_{ms} decreases at a rate similar to $(Rb_{1-x}K_x)_{0.3}MoO_3$. A crystal with 37.7% Cs shows a 12° decrease in the resistive T_{ms} compared to $Rb_{0.3}MoO_3$ (168 K versus 180 K, respectively) (Fig. 2). The differential magnetic susceptibility displays the same decrease in T_{ms} upon Cs substitution (Fig. 3).

It is surprising that the resistivity at room temperature decreases by roughly an order of magnitude with ~40% Cs substitution (Table IV). Although there is about a 20% error in the resistivity values due to uncertainty in crystal size and the finite size of the voltage contacts this cannot account for the large decrease in ρ (298 K). These results have been confirmed by the measurement of ~20 different crystals of varying cesium composition. Samples selected for measurement were usually cleaved and examined for impurities. The most common impurity found was $Cs_{0.33}MoO_3$. If this compound were present ρ would be expected to increase since $Cs_{0.33}MoO_3$ has ρ (298 K) ~ 10^5 Ω cm (*22*). Only "pure" crystals were measured. A final note is that there was no mention of an enhancement of the conductivity in $(Rb_{1-x}K_x)_{0.3}MoO_3$ crystals (*10*).

It appears that cesium could change the transport properties of $Rb_{0.3}MoO_3$ through its large size. The *d*-spacing for the 201 reflection increases from 8.31 to 8.55 Å for $Rb_{0.3}MoO_3$ and $(Rb_{0.55}Cs_{0.45})_{0.3}MoO_3$, respectively. As Cs replaces Rb, the distance between the MoO_6 octahedral slabs increases. As expected, *a*, *c*, β, and the cell volume increase (Table III, Fig. 1). The monoclinic *b* axis remains essentially unchanged. As the Cs content increases, the "electronic isolation" of the Mo–O sheets seem to be larger. It is plausible that this effect will increase the low-dimensionality of the system. An increase in charge carriers along *b* would result in decreased resistivity. The increase in the ratio of ρ (298 K) perpendicular to *b* and $(\bar{2}01)$ to ρ (298 K)

parallel to *b* with increasing Cs content lends some support for this hypothesis. Hall measurements on oriented crystals along these two directions might clarify this issue. Since *b* remains nearly constant, better orbital overlap along this direction cannot be used to argue for the increased conduction. The resistivity in the perpendicular direction actually shows a slight decrease with increasing Cs content (Table IV). However, the configuration of the electrode contacts for this measurement increases the likelihood of current leakage along *b* which could lead to the observed trend in the resistivity.

In summary, the results of substitution in the $(Rb_{1-x}Cs_x)_{0.3}MoO_3$ system are comparable to that found for $(Rb_{1-x}K_x)_{0.3}MoO_3$ except for the decreased resistivity exhibited by the former. The origin of this effect is presently unclear. A study of the temperature dependence of χ in several crystallographic directions would be useful in further attempting to clarify the behavior observed in $(Rb_{1-x}Cs_x)_{0.3}MoO_3$. Oriented magnetic measurements on $K_{0.3}MoO_3$ (*20*) show a susceptibility anisotropy approximately a factor of 1.1 in the (201) plane and a factor of 2.5 between these planes. It would be of interest to see if the increased anisotropy found in the resistivity for $(Rb_{1-x}Cs_x)_{0.3}MoO_3$ crystals is also present in the susceptibility.

Acknowledgments

We gratefully acknowledge Mark Greaney for atomic absorption measurements. This research was supported by National Science Foundation Solid State Chemistry Grants DMR-84-04003 and DMR-87-14072 and National Science Foundation Materials Research Instrumentation Grants DMR-84-08266 and DMR-87-05620.

References

1. G. Travaglini, P. Wachter, J. Marcus, and C. Schlenker, *Solid State Commun.* **37,** 599 (1981).
2. J. P. Pouget, S. Kagoshima, C. Schlenker, and J. Marcus, *J. Phys. Lett.* **44,** L-113 (1983).
3. J. Dumas, C. Schlenker, J. Marcus, and R. Buder, *Phys. Rev. Lett.* **50,** 757 (1983).
4. C. Schlenker, C. Filippini, J. Marcus, J. Dumas, J. P. Pouget, and S. Kagoshima, *J. Phys. C* **44,** 1757 (1983).
5. R. J. Cava, R. M. Fleming, P. B. Littlewood, E. A. Rietman, L. F. Schneemeyer, and R. G. Dunn, *Phys. Rev. B* **30,** 3228 (1984).
6. J. Dumas, A. Arbaoni, J. Marcus, and C. Schlenker, *Mol. Cryst. Liq. Cryst.* **121,** 117 (1985).
7. J. Graham and A. D. Wadsley, *Acta Crystallogr.* **20,** 93 (1966).
8. M. Ghedira, J. Chenovas, M. Marezio, and J. Marcus, *J. Solid State Chem.* **57,** 300 (1985).
9. M. Ganne, A. Boumaza, M. Dion, and J. Dumas, *Mater. Res. Bull.* **20,** 1297 (1985).
10. L. F. Schneemeyer, F. J. DiSalvo, S. E. Spengler, and J. V. Waszczak, *Phys. Rev. B* **30,** 4297 (1984).
11. L. F. Schneemeyer, R. M. Fleming, and S. E. Spengler, *Solid State Commun.* **53,** 505 (1985).
12. R. J. Cava, L. F. Schneemeyer, R. M. Fleming, P. B. Littlewood, and E. A. Rietman, *Phys. Rev. B* **32,** 4088 (1985).
13. W. H. McCarroll and M. Greenblatt, *J. Solid State Chem.* **54,** 282 (1984).
14. K. V. Ramanujachary, M. Greenblatt, and W. H. McCarroll, *J. Cryst. Growth* **70,** 476 (1984).
15. K. V. Ramanujachary, B. T. Collins, M. Greenblatt, P. McNally, and W. H. McCarroll, *Solid State Ionics* **22,** 105 (1986).
16. B. T. Collins, K. V. Ramanujachary, M. Greenblatt, W. H. McCarroll, P. McNally, and J. V. Waszczak, *J. Solid State Chem.* **76,** 319 (1988).
17. F. J. DiSalvo and J. V. Waszczak, *Phys. Rev. B* **23,** 457 (1981).
18. P. Beauchene, J. Dumas, A. Janossy, J. Marcus, and C. Schlenker, *Phys. B & C* **143,** 126 (1986).
19. B. T. Collins, K. V. Ramanujachary, M. Greenblatt, and J. V. Waszczak, *Solid State Commun.* **56,** 1023 (1985).
20. L. F. Schneemeyer, F. J. DiSalvo, R. M. Fleming, and J. V. Waszczak, *J. Solid State Chem.* **54,** 358 (1984).
21. J. T. DeVreese *et al.* (Eds.), "Highly Conducting One-Dimensional Solids," Plenum, New York (1979).
22. P. Strobel and M. Greenblatt, *J. Solid State Chem.* **36,** 331 (1981).